

Proton radii for muonic hydrogen spectroscopy from lattice QCD

Miguel Salg,^{a,b,*} Dalibor Djukanovic,^{c,d} Georg von Hippel,^b Harvey B. Meyer,^{b,c}
Konstantin Ottnad^b and Hartmut Wittig^{b,c}

^aAlbert Einstein Center for Fundamental Physics, Institute for Theoretical Physics, University of Bern,
Sidlerstrasse 5, 3012 Bern, Switzerland

^bPRISMA⁺ Cluster of Excellence and Institute for Nuclear Physics, Johannes Gutenberg University Mainz,
Johann-Joachim-Becher-Weg 45, 55128 Mainz, Germany

^cHelmholtz Institute Mainz, Staudingerweg 18, 55128 Mainz, Germany

^dGSI Helmholtzzentrum für Schwerionenforschung, 64291 Darmstadt, Germany

E-mail: msalg@uni-mainz.de

The size of the proton is of lasting and high interest in the subatomic physics community. The most well-known example is the electric radius which has been the subject of the proton radius puzzle for more than a decade. While tremendous progress in ep -scattering, atomic spectroscopy, and lattice QCD has brought this puzzle closer to its resolution, one also finds discrepant results for the magnetic radius. In light of the upcoming high-precision measurements of the hyperfine splitting (HFS) in muonic hydrogen, other definitions of radii gain relevance as well. On the one hand, to infer the electric radius from the observed Lamb shift in muonic hydrogen, higher-order nuclear structure corrections need to be subtracted, which depend on the Friar radius of the proton. The magnetic properties of the proton, on the other hand, only enter the HFS via the proton's Zemach radius. Based on our previous calculation of the electromagnetic form factors of the proton and neutron, which includes both quark-connected and -disconnected contributions and assesses all sources of systematic uncertainties, we now present results for the Zemach and Friar radii. For the proton, we obtain $r_Z^p = (1.013 \pm 0.010 \text{ (stat)} \pm 0.012 \text{ (syst)})$ fm and $r_F^p = (1.301 \pm 0.012 \text{ (stat)} \pm 0.014 \text{ (syst)})$ fm. These numbers suggest small values of the Zemach and Friar radii of the proton, and have a precision which is sufficient to make a meaningful comparison to data-driven evaluations.

MITP-24-072

The 41st International Symposium on Lattice Field Theory (LATTICE2024)
28 July - 3 August 2024
Liverpool, UK

*Speaker

1. Introduction

The most accurate determination of the proton’s electric (charge) radius is derived from the measurement of the Lamb shift in muonic hydrogen spectroscopy [1, 2]. This result exhibits a large tension with some ep -scattering experiments [3, 4], which is known as the “proton radius puzzle”.

To infer the electric radius from the observed Lamb shift, higher-order nuclear structure-contributions need to be subtracted. The leading contribution is the two-photon exchange [5], the dominant, elastic part of which depends on the third Zemach moment of the proton [6–8],

$$\langle r_E^3 \rangle_{(2)}^P = \frac{24}{\pi} \int_0^\infty \frac{dQ^2}{(Q^2)^{5/2}} \left[(G_E^P(Q^2))^2 - 1 + \frac{1}{3} \langle r_E^2 \rangle^P Q^2 \right]. \quad (1)$$

The associated radius is known as the Friar radius of the proton, $r_F^P = \sqrt[3]{\langle r_E^3 \rangle_{(2)}^P}$.

While the traditional proton radius puzzle awaits its final resolution, the goal of reaching a consistent picture of all the fundamental electromagnetic properties of the nucleon has attained a new prominence. For the magnetic radius, for instance, a tension between dispersive approaches [9] and z -expansion results [10] appeared, *i.e.*, a separate puzzle beclouds the magnetic properties of the proton. Underlining the importance of the magnetic properties of the proton, several experiments are under way to measure these from spectroscopy on (muonic) hydrogen [11–14]. This can be achieved by measuring, in addition to the Lamb shift, the hyperfine splitting (HFS).

The leading-order proton-structure contribution to the S -state HFS of hydrogen depends on the Zemach radius of the proton [7, 15],

$$r_Z^P = -\frac{2}{\pi} \int_0^\infty \frac{dQ^2}{(Q^2)^{3/2}} \left[\frac{G_E^P(Q^2)G_M^P(Q^2)}{\mu_M^P} - 1 \right]. \quad (2)$$

Having a first-principles prediction of r_Z^P prior to the experimental measurement of the ground-state (1S) HFS in muonic hydrogen with ppm precision [11–14], from which the Zemach radius could be extracted with sub-percent uncertainty, is highly desirable. Beyond helping in narrowing down the frequency search range, such a prediction allows for a crucial consistency check.

In this contribution, we present our lattice-QCD calculation of the Zemach and Friar radii, building on our results for the electromagnetic radii of the proton and neutron [16, 17]. Our results for the Zemach and Friar radii of the proton have a total precision of 1.5 %, and are well compatible with most of the experimental determinations [2, 9, 10, 18–20]. This presentation is based on Ref. [21], to which we refer the interested reader for further details.

2. Lattice setup

In order to compute the Zemach and Friar radii of the proton and neutron, we need, according to Eqs. (1) and (2), information on their electric and magnetic form factors. For our lattice determination of the latter, we employ a set of ensembles with $N_f = 2 + 1$ flavors of non-perturbatively $\mathcal{O}(a)$ -improved Wilson fermions [22, 23], using the tree-level improved Lüscher-Weisz gluon action [24], which have been generated as part of the Coordinated Lattice Simulations (CLS) effort [25]. The ensembles entering our analysis are listed in Table 1 and cover four

lattice spacings $a \in [0.050, 0.086]$ fm, as well as several pion masses down to slightly below the physical one (E250). We include the contributions from quark-connected as well as -disconnected diagrams. For further details concerning the setup of the simulations, the calculation of our raw lattice observables, the extraction of the form factors, and the treatment of excited states, we refer to Ref. [16].

ID	β	t_0^{sym}/a^2	T/a	L/a	M_π [MeV]
C101	3.40	2.860(11)	96	48	227
N101 ^a	3.40	2.860(11)	128	48	283
H105 ^a	3.40	2.860(11)	96	32	283
D450	3.46	3.659(16)	128	64	218
N451 ^a	3.46	3.659(16)	128	48	289
E250	3.55	5.164(18)	192	96	130
D200	3.55	5.164(18)	128	64	207
N200 ^a	3.55	5.164(18)	128	48	281
S201 ^a	3.55	5.164(18)	128	32	295
E300	3.70	8.595(29)	192	96	176
J303	3.70	8.595(29)	192	64	266

^aThese ensembles are not used in the final fits but only to constrain discretization and finite-volume effects.

Table 1: Overview of the ensembles used in this study. For further details, see Table I of Ref. [16].

All dimensionful quantities are expressed in units of the gradient flow time t_0 [26]. To this end, we use the numerical determination at the flavor-symmetric point, t_0^{sym}/a^2 , from Ref. [27]. Only our final results for the radii are converted to physical units using the FLAG estimate for $N_f = 2 + 1$, $\sqrt{t_{0,\text{phys}}} = 0.14464(87)$ fm [28].

3. Fits to baryonic χ PT

In Refs. [16, 17] we have combined the parametrization of the Q^2 -dependence of the form factors with the extrapolation to the physical point ($M_\pi = M_{\pi,\text{phys}}$, $a = 0$, $L = \infty$). For this purpose, we have fitted our form factor data to the next-to-leading-order expressions resulting from covariant baryon chiral perturbation theory (B χ PT) [29]. While explicit Δ degrees of freedom are not considered in the fit, we include the contributions from the relevant vector mesons, as discussed in detail in Ref. [16]. For the physical pion mass we use the value in the isospin limit [30].

We perform several such fits, applying different cuts in the pion mass ($M_\pi \leq 0.23$ GeV and $M_\pi \leq 0.27$ GeV) and the momentum transfer ($Q^2 \leq 0.3, \dots, 0.6$ GeV²), and, at the same time, varying our model for the lattice-spacing and/or finite-volume dependence, in order to estimate the corresponding systematic uncertainties. The relatively strict cuts in Q^2 are required because the B χ PT expansion, from which our fit formulae are derived, is only applicable for low momentum transfers. By including the contributions from vector mesons, the range of validity of the resulting expressions can be extended [29, 31, 32]. Nevertheless, as the heaviest vector meson we consider

in the isovector channel is the ρ , momentum transfers larger than $M_\rho^2 \approx 0.6 \text{ GeV}^2$ cannot safely be described in this way. For further details on the $B\chi$ PT fits and an extensive cross-check of our excited-state analysis as well as of the parametrization of the Q^2 -dependence and the extrapolation to the physical point, we refer to Ref. [16].

4. Extrapolation of the form factors and integration

Given that the Zemach radius and third Zemach moment are defined as integrals over all values of $Q^2 \in (0, \infty)$ [cf., Eqs. (1) and (2)], an extrapolation of the $B\chi$ PT fits beyond their range of applicability is required if they are to be employed to parametrize the form factors. For each model, we evaluate the $B\chi$ PT formula for $G_E^{p,n}$ and $G_M^{p,n}$, using the low-energy constants as determined from the corresponding fit, at the physical point and at 20 evenly spaced points in $Q^2 \in [0, Q_{\text{cut}}^2]$. Here, Q_{cut}^2 is the cut in the momentum transfer corresponding to the respective $B\chi$ PT fit variation.

Next, we fit a model which obeys the perturbative large- Q^2 constraints on the form factors [33] to these data points and their error estimates, using the model-independent z -expansion [34],

$$G_E^{p,n}(Q^2) = \sum_{k=0}^m a_k^{p,n} z(Q^2)^k, \quad G_M^{p,n}(Q^2) = \sum_{k=0}^m b_k^{p,n} z(Q^2)^k, \quad (3)$$

with

$$z(Q^2) = \frac{\sqrt{\tau_{\text{cut}} + Q^2} - \sqrt{\tau_{\text{cut}} - \tau_0}}{\sqrt{\tau_{\text{cut}} + Q^2} + \sqrt{\tau_{\text{cut}} - \tau_0}}, \quad (4)$$

where we employ $\tau_0 = 0$ and $\tau_{\text{cut}} = 4M_{\pi,\text{phys}}^2$. We truncate the z -expansion beyond $m = 9$, and incorporate the four sum rules from Ref. [35] for each form factor, which ensure the correct asymptotic behavior of the latter for large Q^2 . The normalization of the electric form factor is enforced by fixing $a_0^p = 1$ and $a_0^n = 0$, respectively. For the determination of the Zemach radius, we fit G_E and G_M simultaneously, while for the third Zemach moment, where G_M is not required, we fit only G_E . The extrapolation fits are performed for the proton and neutron independently. Using more than 20 data points for each form factor or a higher degree of the z -expansion does not increase the overlap between the original $B\chi$ PT fit and the extrapolation any further.

For the numerical integration of Eqs. (1) and (2), we smoothly replace the $B\chi$ PT parametrization of the form factors by the z -expansion-based extrapolation in a narrow window around Q_{cut}^2 . Concretely, we use the following *ansatz* to estimate the form factor term,

$$F(Q^2) = \frac{1}{2} \left[1 - \tanh \left(\frac{Q^2 - Q_{\text{cut}}^2}{\Delta Q_w^2} \right) \right] F^\chi(Q^2) + \frac{1}{2} \left[1 + \tanh \left(\frac{Q^2 - Q_{\text{cut}}^2}{\Delta Q_w^2} \right) \right] F^z(Q^2), \quad (5)$$

where $F(Q^2) \equiv G_E(Q^2)G_M(Q^2)/\mu_M$ for the Zemach radius and $F(Q^2) \equiv G_E^2(Q^2)$ for the third Zemach moment, respectively. In Eq. (5), $F^\chi(Q^2)$ represents our fit to $B\chi$ PT, while $F^z(Q^2)$ denotes the z -expansion parametrization of the form factors. For the width of the window in which we switch between the two parametrizations, we choose $\Delta Q_w^2 = 0.0537t_0^{-1} \approx 0.1 \text{ GeV}^2$. We remark that the cancellation between the different terms of Eq. (1) at small Q^2 does not occur at the required numerical accuracy on all our bootstrap samples. To facilitate the numerical integration, we therefore

regulate the small- Q^2 contribution to the integral for the proton by replacing $t_0 Q^2 \rightarrow t_0 Q^2 + 1 \times 10^{-7}$ in the denominator, which changes the result for $\langle r_E^3 \rangle_{(2)}^P$ by less than 6 % of its statistical error.

The two parametrizations and their weighted average according to Eq. (5) are illustrated in Fig. 1 for the case of the Zemach radius. While the breakdown of the $B\chi$ PT formula is clearly visible, the z -expansion behaves well for arbitrarily large momenta, which is due to the sum rules [35] we have included. However, in the region where we adjust the z -expansion to the $B\chi$ PT parametrization ($0 \leq Q^2 \leq 0.6 \text{ GeV}^2$ for the case shown in Fig. 1), the two curves overlap extremely well. The blue curve, which is the one we use for the integration, smoothly switches from the orange ($B\chi$ PT) curve to the gray (z -expansion) one in a tight window around $Q_{\text{cut}}^2 = 0.6 \text{ GeV}^2 = 0.322 t_0^{-1}$.

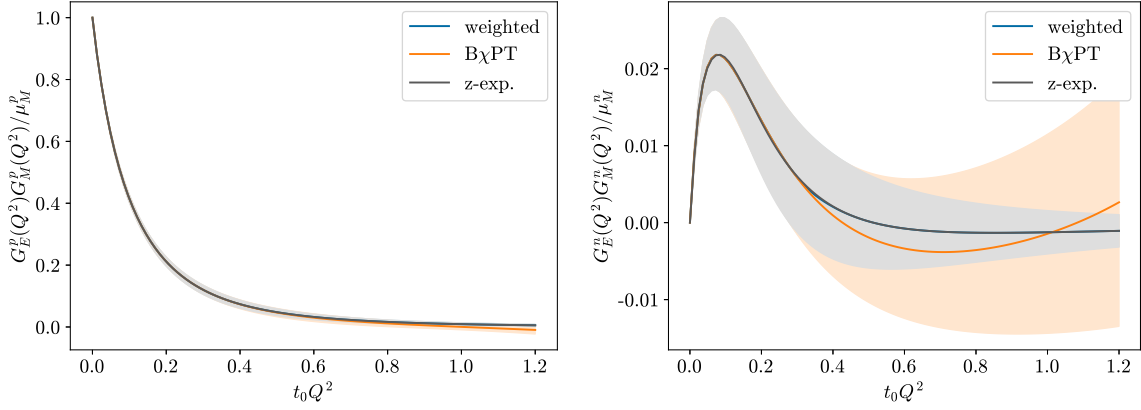


Figure 1: Product of the electric and normalized magnetic form factors of the proton (left panel) and neutron (right panel) at the physical point evaluated with different parametrizations. The orange curve shows one of the $B\chi$ PT fits to our lattice data with $Q_{\text{cut}}^2 = 0.6 \text{ GeV}^2 \approx 0.322 t_0^{-1}$, the gray curve the z -expansion-based extrapolation, and the blue curve the weighted average of the two according to Eq. (5).

Replacing the $B\chi$ PT parametrization smoothly with a constant zero instead of the z -expansion-based extrapolation [*i.e.*, setting $F^z(Q^2) \equiv 0$ in Eq. (5)] allows one to estimate the contribution of the form factors at $Q^2 > Q_{\text{cut}}^2$ to the full integrals. For $Q_{\text{cut}}^2 = 0.6 \text{ GeV}^2$ (our largest, *i.e.*, least stringent, value for the cut), we find that the relative difference of the thus obtained value for r_Z^P ($\langle r_E^3 \rangle_{(2)}^P$) to the full result using the corresponding variation of the $B\chi$ PT fits is less than 0.9 % (0.3 %). In other words, the form factor terms at $Q^2 > 0.6 \text{ GeV}^2$ contribute less than 0.9 % (0.3 %) to the proton’s Zemach radius (third Zemach moment).

Finally, we note that the major advantage of our approach based on the $B\chi$ PT fits over an integration of the form factors on each ensemble is that the Zemach and Friar radii can be computed directly at the physical point, so that an extrapolation of results for the radii to the physical point, which would entail further significant systematic uncertainties, is not required.

5. Model average and final result

As in Refs. [16, 17], we do not have a strong *a priori* preference for one specific setup of the $B\chi$ PT fits. Thus, we determine our final results as well as the statistical and systematic error estimates from an average over the different fit models and kinematic cuts, using weights derived

from the Akaike Information Criterion (AIC) [36–41]. More details on our procedure can be found in section V of Ref. [16]. As our final results, we obtain

$$r_Z^p = (1.013 \pm 0.010 \text{ (stat)} \pm 0.012 \text{ (syst)}) \text{ fm}, \quad (6)$$

$$\langle r_E^3 \rangle_{(2)}^p = (2.200 \pm 0.060 \text{ (stat)} \pm 0.071 \text{ (syst)}) \text{ fm}^3, \quad (7)$$

$$r_Z^n = (-0.0411 \pm 0.0056 \text{ (stat)} \pm 0.0040 \text{ (syst)}) \text{ fm}, \quad (8)$$

$$\langle r_E^3 \rangle_{(2)}^n = (0.0078 \pm 0.0020 \text{ (stat)} \pm 0.0012 \text{ (syst)}) \text{ fm}^3. \quad (9)$$

This corresponds to Friar radii of $r_F^p = (1.301 \pm 0.012 \text{ (stat)} \pm 0.014 \text{ (syst)}) \text{ fm}$ and $r_F^n = (0.198 \pm 0.017 \text{ (stat)} \pm 0.010 \text{ (syst)}) \text{ fm}$, respectively.

In Fig. 2, our numbers for the proton are compared to other determinations based on experimental data. There are three main types of experiments which have been employed in the literature to compute the Zemach radius of the proton: muonic hydrogen HFS [2], electronic hydrogen HFS [42], and ep scattering. In order to extract the proton Zemach radius from an HFS measurement, input on the proton-polarizability effect is required. This can be either taken from $B\chi$ PT [20] or evaluated in a data-driven fashion, *i.e.*, using information on the spin structure functions [43–45] (as was done in Refs. [2, 18]). The form factors measured in ep -scattering experiments, on the other hand, can be analyzed with many different fit models, *e.g.*, by employing a (modified) power series [19], a z -expansion [10], or dispersion theory [9].

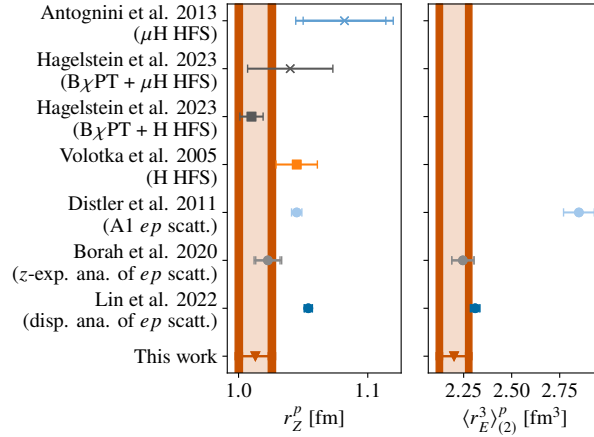


Figure 2: Comparison of our best estimates for the Zemach radius and third Zemach moment of the proton (red downward-pointing triangles) with determinations based on experimental data, *i.e.*, muonic hydrogen HFS [2, 20] (crosses), electronic hydrogen HFS [18, 20] (squares), and ep scattering [9, 10, 19] (circles).

While our result for r_Z^p agrees within two combined standard deviations with most of the data-driven extractions [2, 10, 18–20], we observe a 2.6σ tension with the dispersive analysis of world ep -scattering data [9]. We also note that our estimate for r_Z^p is smaller than almost all of the experimental determinations. The proton’s third Zemach moment can be extracted from ep -scattering experiments in the same way as its Zemach radius, and we also compare to these results in Fig. 2. Again, our value is comparatively small, but this time in good agreement with both the z -expansion-based [10] and dispersive analyses [9]. Against the analysis of the A1 ep -scattering experiment [19], on the other hand, we observe a clear tension of 5.3σ in $\langle r_E^3 \rangle_{(2)}^p$.

In interpreting the aforementioned discrepancies, one must take into account that our results for the Zemach radii and third Zemach moments are not independent from those for the electromagnetic radii [16, 17] because they are based on the same lattice data for the form factors and the same $B\chi$ PT fits. To quantify this correlation, we estimate the covariance matrix of our model-averaged results for the different proton radii r_j ,

$$C_{jk} = \frac{1}{(\text{cdf}_{\mathcal{N}}^{-1}(3/4))^2} \text{med}([r_j - \text{med}(r_j)][r_k - \text{med}(r_k)]), \quad \text{corr}_{jk} = C_{jk}/\sqrt{C_{jj}C_{kk}}, \quad (10)$$

where $\text{cdf}_{\mathcal{N}}^{-1}$ denotes the inverse cumulative distribution function (CDF) of a Gaussian distribution, and the median is calculated from the model-averaged (empirical) CDF. For the correlation matrix of $[\sqrt{\langle r_E^2 \rangle^p}, \sqrt{\langle r_M^2 \rangle^p}, r_Z^p, r_F^p]$, we thus obtain

$$\text{corr} = \begin{pmatrix} 1 & 0.41294995 & 0.85702489 & 0.97214447 \\ 0.41294995 & 1 & 0.72010978 & 0.42834371 \\ 0.85702489 & 0.72010978 & 1 & 0.79974042 \\ 0.97214447 & 0.42834371 & 0.79974042 & 1 \end{pmatrix}. \quad (11)$$

Hence, we indeed observe a strong correlation both between $\sqrt{\langle r_E^2 \rangle^p}$ and r_Z^p and between $\sqrt{\langle r_M^2 \rangle^p}$ and r_Z^p , as well as between $\sqrt{\langle r_E^2 \rangle^p}$ and r_F^p . We note that a large positive correlation between the proton's electric and Zemach radii has also been reported in the experimental literature [46, 47].

A selection of the results for r_Z^p and r_F^p from Fig. 2 are plotted against the corresponding values for $\sqrt{\langle r_E^2 \rangle^p}$ and $\sqrt{\langle r_M^2 \rangle^p}$ in Fig. 3. This demonstrates that if a particular analysis yields a larger electric radius, it generally also produces larger Zemach and Friar radii. Approximating the model-averaged distribution in each two-dimensional projection as a multivariate Gaussian in the vicinity of our central values, we can draw confidence ellipses as displayed in Fig. 3. They illustrate again the strong correlation among our lattice results for the different proton radii and show that these confirm the trends observed in the data-driven evaluations as far as the correlation of the Zemach and Friar radii with the electric radius is concerned.

We conclude that our small results for $\sqrt{\langle r_E^2 \rangle^p}$ and $\sqrt{\langle r_M^2 \rangle^p}$ in Refs. [16, 17] naturally imply small values for r_Z^p and r_F^p . By contrast, dispersive analyses like Ref. [9] arrive at a significantly larger magnetic radius than the A1-data analyses [3, 35] and our lattice-QCD-based extraction [16, 17]. This may explain why we observe a larger tension in the Zemach radius (which equally probes electric and magnetic properties) with Ref. [9] than with Ref. [19], even though the situation is exactly the opposite for the third Zemach moment / Friar radius (which only probes the electric properties). For a deeper understanding of the underlying differences, a comparison of the full Q^2 -dependence of the form factors would be required, rather than merely of the radii.

Our results for the neutron are very well compatible with the z -expansion-based analysis of world en -scattering data [10], albeit with a more than two times larger error.

6. Conclusions

We have presented our lattice-QCD calculation of the Zemach and Friar radii of the proton and neutron, which includes the contributions from quark-connected and -disconnected diagrams

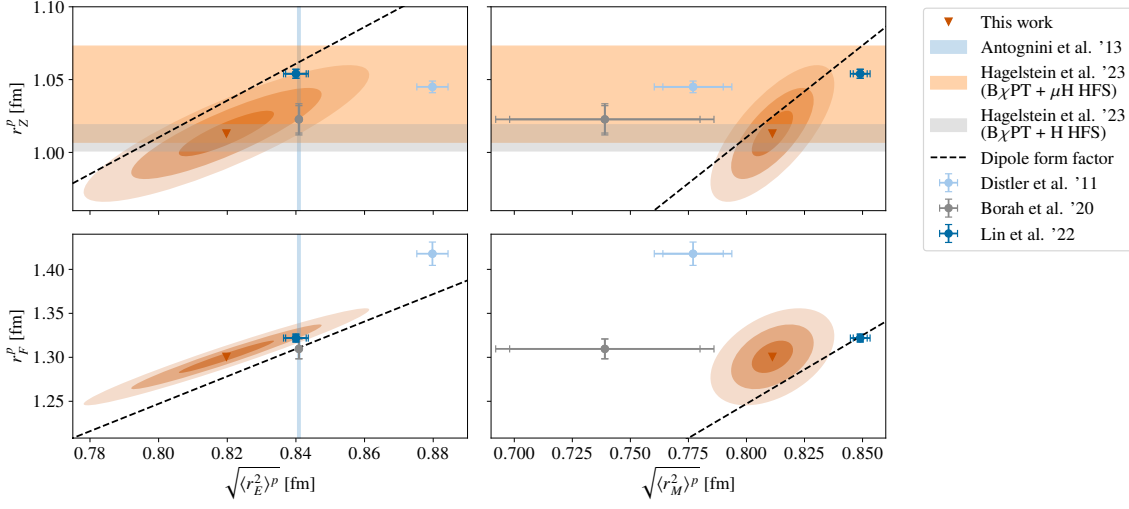


Figure 3: Correlation between the different proton radii. The results of this work (red downward-pointing triangles; shaded ellipses: 1σ , 2σ , and 3σ confidence regions) are compared with determinations based on experimental data (*cf.*, Fig. 2) [2, 9, 10, 19, 20]. The dashed black line is calculated with a dipole form for G_E and G_M assuming the same dipole mass for both form factors, which is varied along the line.

and presents a full error budget. The overall precision of our results for the proton is sufficient to make a meaningful comparison to data-driven evaluations. Our final estimates, which are given in Eqs. (6) to (9), point to small values for the Zemach and Friar radii of the proton, but are consistent with most of the previous determinations within two standard deviations. While they do not give rise to an independent puzzle from the lattice perspective, they emphasize that we agree rather well with the dispersive analysis of Ref. [9] regarding the electric properties of the proton (*i.e.*, the Friar radius), but to a much lesser degree on its magnetic properties (*i.e.*, the Zemach radius).

Acknowledgments

We thank Franziska Hagelstein for useful discussions, and Simon Kuberski for providing the improved reweighting factors [48] for the gauge ensembles used in our calculation. Moreover, we are grateful to our colleagues in the CLS initiative for sharing the gauge field configurations on which this work is based. This research is partly supported by the Deutsche Forschungsgemeinschaft (DFG, German Research Foundation) through project HI 2048/1-2 (project No. 399400745) and through the Cluster of Excellence ‘‘Precision Physics, Fundamental Interactions and Structure of Matter’’ (PRISMA⁺ EXC 2118/1) funded within the German Excellence Strategy (project ID 39083149). Calculations for this project were partly performed on the HPC clusters ‘‘Clover’’ and ‘‘HIMster2’’ at the Helmholtz Institute Mainz, and partly using the supercomputer ‘‘Mogon 2’’ operated by Johannes Gutenberg University Mainz, which is a member of the AHRP (Alliance for High Performance Computing in Rhineland Palatinate), the Gauss Alliance e.V., and the NHR Alliance (Nationales Hochleistungsrechnen). We also gratefully acknowledge the John von Neumann Institute for Computing (NIC) and the Gauss Centre for Supercomputing e.V. for funding this project by providing computing time on the GCS Supercomputer JUWELS at Jülich Supercomputing Centre (JSC) through projects CHMZ21, CHMZ36, NUCSTRUCLFL, and GCSNUCL2PT.

References

- [1] R. Pohl et al., *The size of the proton*, *Nature* **466** (2010) 213.
- [2] A. Antognini et al., *Proton structure from the measurement of 2S-2P transition frequencies of muonic hydrogen*, *Science* **339** (2013) 417.
- [3] A1 COLLABORATION, *Electric and magnetic form factors of the proton*, *Phys. Rev. C* **90** (2014) 015206 [1307.6227].
- [4] M. Mihovilović et al., *The proton charge radius extracted from the initial-state radiation experiment at MAMI*, *Eur. Phys. J. A* **57** (2021) 107 [1905.11182].
- [5] K. Pachucki et al., *Comprehensive theory of the Lamb shift in light muonic atoms*, *Rev. Mod. Phys.* **96** (2024) 015001 [2212.13782].
- [6] J.L. Friar, *Nuclear finite-size effects in light muonic atoms*, *Annals Phys.* **122** (1979) 151.
- [7] K. Pachucki, *Theory of the Lamb shift in muonic hydrogen*, *Phys. Rev. A* **53** (1996) 2092.
- [8] K. Pachucki, *Proton structure effects in muonic hydrogen*, *Phys. Rev. A* **60** (1999) 3593 [physics/9906002].
- [9] Y.-H. Lin, H.-W. Hammer and U.-G. Meißner, *New insights into the nucleon's electromagnetic structure*, *Phys. Rev. Lett.* **128** (2022) 052002 [2109.12961].
- [10] K. Borah et al., *Parametrization and applications of the low- Q^2 nucleon vector form factors*, *Phys. Rev. D* **102** (2020) 074012 [2003.13640].
- [11] M. Sato et al., *Laser spectroscopy of the hyperfine splitting energy in the ground state of muonic hydrogen*, in *20th International Conference on Particles and Nuclei*, pp. 460–463, 2014, DOI.
- [12] C. Pizzolotto et al., *The FAMU experiment: muonic hydrogen high precision spectroscopy studies*, *Eur. Phys. J. A* **56** (2020) 185.
- [13] C. Pizzolotto et al., *Measurement of the muon transfer rate from muonic hydrogen to oxygen in the range 70-336 K*, *Phys. Lett. A* **403** (2021) 127401 [2105.06701].
- [14] P. Amaro et al., *Laser excitation of the 1s-hyperfine transition in muonic hydrogen*, *SciPost Phys.* **13** (2022) 020 [2112.00138].
- [15] A.C. Zemach, *Proton structure and the hyperfine shift in hydrogen*, *Phys. Rev.* **104** (1956) 1771.
- [16] D. Djukanovic et al., *Electromagnetic form factors of the nucleon from $N_f = 2 + 1$ lattice QCD*, *Phys. Rev. D* **109** (2024) 094510 [2309.06590].
- [17] D. Djukanovic et al., *Precision calculation of the electromagnetic radii of the proton and neutron from lattice QCD*, *Phys. Rev. Lett.* **132** (2024) 211901 [2309.07491].

- [18] A.V. Volotka et al., *Zemach and magnetic radius of the proton from the hyperfine splitting in hydrogen*, *Eur. Phys. J. D* **33** (2005) 23 [[physics/0405118](#)].
- [19] M.O. Distler, J.C. Bernauer and T. Walcher, *The RMS charge radius of the proton and Zemach moments*, *Phys. Lett. B* **696** (2011) 343 [[1011.1861](#)].
- [20] F. Hagelstein, V. Lensky and V. Pascalutsa, *Chiral perturbation theory of the hyperfine splitting in (muonic) hydrogen*, *Eur. Phys. J. C* **83** (2023) 762 [[2305.09633](#)].
- [21] D. Djukanovic et al., *Zemach and Friar radii of the proton and neutron from lattice QCD*, *Phys. Rev. D* **110** (2024) L011503 [[2309.17232](#)].
- [22] B. Sheikholeslami and R. Wohlert, *Improved continuum limit lattice action for QCD with Wilson fermions*, *Nucl. Phys. B* **259** (1985) 572.
- [23] J. Bulava and S. Schaefer, *Improvement of $N_f = 3$ lattice QCD with Wilson fermions and tree-level improved gauge action*, *Nucl. Phys. B* **874** (2013) 188 [[1304.7093](#)].
- [24] M. Lüscher and P. Weisz, *On-shell improved lattice gauge theories*, *Comm. Math. Phys.* **97** (1985) 59, Erratum *ibid.* **98** (1985) 433.
- [25] M. Bruno et al., *Simulation of QCD with $N_f = 2 + 1$ flavors of non-perturbatively improved Wilson fermions*, *JHEP* **02** (2015) 43 [[1411.3982](#)].
- [26] M. Lüscher, *Properties and uses of the Wilson flow in lattice QCD*, *JHEP* **08** (2010) 71 [[1006.4518](#)], Erratum *ibid.* **03** (2014) 92.
- [27] M. Bruno, T. Korzec and S. Schaefer, *Setting the scale for the CLS 2 + 1 flavor ensembles*, *Phys. Rev. D* **95** (2017) 074504 [[1608.08900](#)].
- [28] FLAVOUR LATTICE AVERAGING GROUP, *FLAG Review 2021*, *Eur. Phys. J. C* **82** (2022) 869 [[2111.09849](#)].
- [29] T. Bauer, J.C. Bernauer and S. Scherer, *Electromagnetic form factors of the nucleon in effective field theory*, *Phys. Rev. C* **86** (2012) 065206 [[1209.3872](#)].
- [30] FLAG WORKING GROUP, *Review of lattice results concerning low-energy particle physics*, *Eur. Phys. J. C* **74** (2014) 2890 [[1310.8555](#)].
- [31] B. Kubis and U.-G. Meißner, *Low-energy analysis of the nucleon electromagnetic form factors*, *Nucl. Phys. A* **679** (2001) 698 [[hep-ph/0007056](#)].
- [32] M.R. Schindler, J. Gegelia and S. Scherer, *Electromagnetic form factors of the nucleon in chiral perturbation theory including vector mesons*, *Eur. Phys. J. A* **26** (2005) 1 [[nucl-th/0509005](#)].
- [33] G.P. Lepage and S.J. Brodsky, *Exclusive processes in perturbative quantum chromodynamics*, *Phys. Rev. D* **22** (1980) 2157.

- [34] R.J. Hill and G. Paz, *Model-independent extraction of the proton charge radius from electron scattering*, *Phys. Rev. D* **82** (2010) 113005 [1008.4619].
- [35] G. Lee, J.R. Arrington and R.J. Hill, *Extraction of the proton radius from electron-proton scattering data*, *Phys. Rev. D* **92** (2015) 013013 [1505.01489].
- [36] H. Akaike, *Information theory and an extension of the maximum likelihood principle*, in *Proceedings of the 2nd International Symposium on Information Theory*, B.N. Petrov and F. Csaki, eds., (Budapest), pp. 267–281, Akadémiai Kiadó, 1973.
- [37] H. Akaike, *A new look at the statistical model identification*, *IEEE Trans. Autom. Contr.* **19** (1974) 716.
- [38] E.T. Neil and J.W. Sitison, *Improved information criteria for Bayesian model averaging in lattice field theory*, *Phys. Rev. D* **109** (2024) 014510 [2208.14983].
- [39] K.P. Burnham and D.R. Anderson, *Multimodel inference: Understanding AIC and BIC in model selection*, *Sociological Methods & Research* **33** (2004) 261.
- [40] S. Borsányi et al., *Ab initio calculation of the neutron-proton mass difference*, *Science* **347** (2015) 1452 [1406.4088].
- [41] S. Borsányi et al., *Leading hadronic contribution to the muon magnetic moment from lattice QCD*, *Nature* **593** (2021) 51 [2002.12347].
- [42] H. Hellwig et al., *Measurement of the unperturbed hydrogen hyperfine transition frequency*, *IEEE Trans. Instrum. Meas.* **19** (1970) 200.
- [43] R.N. Faustov and A.P. Martynenko, *Proton-polarizability contribution to the hyperfine splitting in hydrogen*, *Phys. Atom. Nuclei* **65** (2002) 265 [hep-ph/0007044].
- [44] E.V. Cherednikova, R.N. Faustov and A.P. Martynenko, *Proton polarizability contribution to the hyperfine splitting in muonic hydrogen*, *Nucl. Phys. A* **703** (2002) 365 [hep-ph/0108044].
- [45] C.E. Carlson, V. Nazaryan and K. Griffioen, *Proton-structure corrections to hyperfine splitting in muonic hydrogen*, *Phys. Rev. A* **83** (2011) 042509 [1101.3239].
- [46] J.L. Friar and I. Sick, *Comment on “Constraints on Proton Structure from Precision Atomic-Physics Measurements”*, *Phys. Rev. Lett.* **95** (2005) 049101 [nucl-th/0503020].
- [47] A. Antognini, F. Hagelstein and V. Pascalutsa, *The proton structure in and out of muonic hydrogen*, *Ann. Rev. Nucl. Part. Sci.* **72** (2022) 389 [2205.10076].
- [48] S. Kuberski, *Low-mode deflation for twisted-mass and RHMC reweighting in lattice QCD*, *Comput. Phys. Commun.* **300** (2024) 109173 [2306.02385].